LBL-14952
Preprint c.2

Lawrence Berkeley Laboratory

UNIVERSITY OF CALIFORNIA

RECEIVED
LAWRENCE
BERKELEY LABORATORY

SEP 30 1982

LIBRARY AND
DOCUMENTS SECTION

Materials & Molecular Research Division

Submitted to the Journal of Chemical Physics

MULTIPROPERTY EMPIRICAL INTERATOMIC POTENTIALS FOR ArXe AND KrXe[a)]

R.T. Pack, J.J. Valentini, C.H. Becker,
R.J. Buss, and Y.T. Lee

September 1982

TWO-WEEK LOAN COPY

This is a Library Circulating Copy which may be borrowed for two weeks. For a personal retention copy, call Tech. Info. Division, Ext. 6782

Prepared for the U.S. Department of Energy under Contract DE-AC03-76SF00098

LBL-14952 c.2

DISCLAIMER

This document was prepared as an account of work sponsored by the United States Government. While this document is believed to contain correct information, neither the United States Government nor any agency thereof, nor the Regents of the University of California, nor any of their employees, makes any warranty, express or implied, or assumes any legal responsibility for the accuracy, completeness, or usefulness of any information, apparatus, product, or process disclosed, or represents that its use would not infringe privately owned rights. Reference herein to any specific commercial product, process, or service by its trade name, trademark, manufacturer, or otherwise, does not necessarily constitute or imply its endorsement, recommendation, or favoring by the United States Government or any agency thereof, or the Regents of the University of California. The views and opinions of authors expressed herein do not necessarily state or reflect those of the United States Government or any agency thereof or the Regents of the University of California.

LBL-14952

MULTIPROPERTY EMPIRICAL INTERATOMIC POTENTIALS FOR ArXe AND KrXe[a)]

R. T. Pack[b)] and J. J. Valentini[c)]
Los Alamos National Laboratory
Los Alamos, NM 87545

and

C. H. Becker,[d)] R. J. Buss, and Y. T. Lee
Materials and Molecular Research Division
Lawrence Berkeley Laboratory and Department of Chemistry
University of California
Berkeley, California 94720

ABSTRACT

Crossed molecular beam measurements of elastic differential cross sections (DCS) for the scattering of Ar and Kr by Xe are reported. Empirical multiparameter M3SV interatomic potentials for the ArXe and KrXe interactions are determined by simultaneously fitting the DCS, viscosities and virial coefficients; the results are the most accurate potentials yet reported for these systems.

a) This work was supported by the Director, Office of Energy Research, Office of Basic Energy Sciences, Chemical Sciences Division of the U.S. Department of Energy under Contract DE-AC03-76SF00098.
b) Theoretical Division, T-12, MS-J569.
c) Chemistry Division, CHM-2, MS-G732.
d) Present address: Molecular Physics Laboratory, SRI International, Menlo Park, CA 94025.

I. INTRODUCTION

In connection with work reported in the following paper,[1] in which anisotropic empirical intermolecular potentials for the $ArSF_6$ and $KrSF_6$ interactions are determined, we decided to first study the ArXe and KrXe systems, the closest spherical analogues to $ArSF_6$ and $KrSF_6$. In this paper we report the most accurate interatomic potentials yet determined for these systems.

Several studies of the van der Waals potentials for the ArXe system[2-5] and the KrXe system [4-6] have been reported in recent years, but none used as wide a variety of high quality data as is used herein, and a recent compilation[7] ranks none of the potentials available for these two systems as better than Class II whereas Class I potentials are available for many of the other noble gas interactions.

In Section II of this paper we report new, high-quality crossed molecular beam measurements of differential cross sections (DCS) for these systems. Then, in Section III we determine the interatomic potentials by simultaneously fitting these DCS data, the accurate viscosity (η) data of Kestin, et. al,[8] and the second virial coefficient (B) data of Brewer[9] and of Rentschler and Schramm.[10]

The three properties (DCS, η, and B) used in the fitting are complementary ones for that purpose. For these pairs of heavy noble gas atoms, the measured DCS at the 64 meV (0.0024 a.u.) relative kinetic energy used is most sensitive to the attractive potential from r_m out to the asymptotic long range region, and the rainbow and supernumerary oscillations give detailed information about that part of the potential. Although η and B show much less structure than the DCS, they have the advantage of being absolute rather than relative values. The η are most sensitive[5] to the wall of the potential from r_m inward to a point where the potential is repulsive by about 1000°K

(0.003 a.u.). The B are sensitive to the size (r_m) of the atoms and to the volume of the attractive well, so that they restrict the way the outer and inner limbs of the potential can be joined together. If any one or two of these three properties are used in the fitting process, one easily fits the data with one or more potentials when flexible forms are used. However, the predictions from the resulting potential for the property or properties not included in the fitting are then usually in error by several times the experimental uncertainties. It is only when all three properties are included in the fitting that the potential is very restricted, and then it requires the full flexibility of the M3SV potential form to fit the three properties within experimental error. This behavior underscores the importance of using several complementary properties if one wishes to determine empirical potentials accurate enough to be used with confidence to predict properties not used in the fitting.

In Section IV we present and discuss our results, and Section V gives our conclusions.

II. EXPERIMENTAL

Elastic differential cross sections for the scattering of Ar and Kr by Xe were obtained by crossing a beam of Ar or Kr with a Xe beam at 90° and measuring the scattered intensity of the Ar or Kr as a function of angle in the plane defined by the beams, using a rotatable, electron impact ionization/quadrupole mass spectrometer detector. The crossed beam apparatus used in these experiments, shown schematically in Figure 1, is discussed only briefly here as it has been described in detail previously.[11]

The Ar, Kr, and Xe beams are each formed by a supersonic free-jet expansion through an 0.10 mm diameter orifice in a quartz nozzle, with a backing pressure of 0.5 to 1.0 atmosphere. Each beam is doubly differentially pumped before entering the scattering chamber. A conical skimmer with a 1.0 mm diameter throat is positioned ~6 mm from the nozzle, between the source and buffer chambers. The primary beam, i.e., the beam of detected Ar or Kr particles, is geometrically defined by a 0.74 mm wide by 1.40 mm high slit between the buffer and scattering chambers, while the secondary beam, Xe, is defined by a second skimmer of diameter 1.70 mm, located between the secondary beam buffer chamber and the scattering chamber. Figure 1 shows these and other details of the geometry of the apparatus used to measure the elastic differential cross sections.

A 150 Hz tuning-fork chopper, located in the secondary beam buffer chamber, modulates the Xe beam. The Ar or Kr atoms which scatter from this modulated Xe beam are synchronously detected by a dual scaler which is locked to the tuning-fork chopper frequency. The scattered Ar or Kr signal thus obtained is integrated for ~40 sec at a given angle. After signal integration at typically 5 angles the detector is moved back to an arbitrarily selected reference angle and the signal here measured. The elastic differen-

tial cross section measurements are then time-normalized with respect to variation in the reference signal, to correct for long-term drift in the experimental apparatus.

The elastic scattering signal is measured at each angle typically 3 to 5 times, in order to improve the signal to noise ratio and also to establish the statistical uncertainty in the measurements. The results of the measurements are shown in Table I for ArXe and in Table II for KrXe. Note that the measurements were made using a nominal laboratory angle which puts the primary beam at -0.4°. This has been corrected so that the tables give the actual laboratory scattering angle from the center of the primary beam.

III. CALCULATIONS

A. M3SV Potential

The interatomic potential we use is an M3SV generalization of the Morse-spline-van der Waals (MSV) form, as sketched in Fig. 2. In regions i = I, II, and III, it is represented by Morse potentials,

$$V_i(r) = \varepsilon_i\{\exp[-2\alpha_i(r-r_{mi})]-2\exp[-\alpha_i(r-r_{mi})]\} \quad . \tag{1}$$

These Morse potentials are chosen so that they are continuous and have continuous first derivatives where they join. Thus, since the boundary of Regions II and III is at r_m, the position of the minimum, one has $\varepsilon_{II} = \varepsilon_{III} = \varepsilon$ and $r_{mII} = r_{mIII} = r_m$, and V_{II} and V_{III} can thus differ only in α_{II} and α_{III}. Similarly, the requirements that

$$V_I(r_o) = V_{II}(r_o) = 0 \quad , \tag{2}$$

and

$$\frac{\partial V_I}{\partial r}\Big|_{r_o} = \frac{\partial V_{II}}{\partial r}\Big|_{r_o} \quad , \tag{3}$$

yield the restrictions that

$$\varepsilon_I = \varepsilon\,\alpha_{II}/\alpha_I \quad , \tag{4}$$

$$r_o = r_m - \alpha_{II}^{-1}\ln 2 \quad , \tag{5}$$

and

$$r_{mI} = r_o + \alpha_I^{-1}\ln 2 \quad , \tag{6}$$

so that α_I is the only independent parameter in V_I.

The potential V is represented in Region IV as a single cubic Hermite spline,

$$V_{IV} = \beta_1 + (x-x_1)\{\beta_2 + (x-x_2)[\beta_3 + (x-x_1)\beta_4]\} \quad , \tag{7}$$

where $x = r/r_m$ is a reduced distance, and in Region V by the asymptotic London or van der Waals expansion,

$$V_V = - C_6 r^{-6} - C_8 r^{-8} - C_{10} r^{-10} \quad . \tag{8}$$

Given V_{III} and V_V, V_{IV} is completely determined by the requirements of continuity of the potential and its slope via

$$\beta_1 = V(x_1) \quad , \tag{9}$$

$$\beta_2 = (x_2-x_1)^{-1}[V(x_2)-\beta_1] \quad , \tag{10}$$

$$\beta_3 = - (x_2-x_1)^{-1}[\partial V/\partial x\big|_{x_1} - \beta_2] \quad , \tag{11}$$

and

$$\beta_4 = (x_2-x_1)^{-1}\{(x_2-x_1)^{-1}[\partial V/\partial x\big|_{x_2} - \beta_2] - \beta_3\} \quad . \tag{12}$$

Thus, although this M3SV form appears to have 18 parameters, only 10 (ε, r_m, α_I, α_{II}, α_{III}, x_1, x_2, and the C_n) are independent, the remaining parameters being determined by the continuity requirements. In practice the 3 C_n are assumed known and varied only if the data cannot be fit otherwise. Similarly, x_1 is usually taken as the inflection point of V_{III},

$$x_1 = r_i/r_m = [r_m + \alpha^{-1}_{III} \ln 2]/r_m \quad , \tag{13}$$

and x_2 is usually held fixed at some value (~1.5) such that r_2 (= $r_m x_2$) is large enough that the series in Eq. (8) is expected to be adequate but small enough to prevent the spline in Eq. (7) from oscillating. Furthermore, in the initial fitting calculations, we use $\alpha = \alpha_I = \alpha_{II} = \alpha_{III}$ (MSV potential) and only allow the α's to become unequal (MMSV or M3SV) if it is necessary to fit the data. Thus, there are really only <u>three</u> parameters (ε, r_m, and α) that are freely varied, with limited or no variation of the others.

The major virtues of the M3SV and related potentials are: (1) They have great flexibility, and (2) the potential can be changed in one region without changing it in another. The major vices are: (1) The potential can have discontinuous second derivatives at the boundaries between regions, and (2) one must "use the tail to wag the dog" in Region IV. That is, as drawn to scale for a typical interaction in Fig. 2, Region IV is rather large, and if ε and r_m are fixed, the potential in that region can only be varied by varying the parameters (α_{III} and the C_n) of Regions III and V. This is important because it is precisely Region IV which dominates in the rainbow scattering of these pairs of large noble gas atoms. The discontinuous second derivative problem is closely related. At most boundaries the discontinuity in $\partial^2 V/\partial r^2$ is small or zero, but at x_1 it can be appreciable, and that is worrisome because it gives the potential no genuine point of inflection, and it is known[12] that the behavior of the potential near the point of inflection is very important to rainbow scattering. To try to improve the potential we also did some calculations with an MQV potential in which a quintic spline assures continuous value, first derivative and second derivative at x_1 and x_2.

However, this turned out to make the transition from Morse to van der Waals behavior occur within a short space located in the middle of Region IV with a sharp unphysical bend in the potential occurring there, and resulted in poorer fits to experiment, so that it was abandoned. Empirical intermolecular potential forms that remove these problems without losing the advantages of MSV-type potentials are needed.

B. Differential Cross Sections

The center of mass differential cross sections (CMDCS) were obtained from the usual formulas[13] using WKB phase shifts calculated via 10-point Gauss-Mehler quadrature[14] at 700 (900) partial waves for ArXe (KrXe). The cross sections were calculated at 211 (220) CM angles at each of 7 CM velocities for ArXe (KrXe) to span the extremes needed in the averaging, and then two dimensional spline interpolation was used to generate the CMDCS at all velocities and angles needed. This procedure was checked and found to be converged with respect to the number of CM velocities and angles used.

For an idealized experiment, the laboratory signal would be proportional to[15]

$$S(\underset{\sim}{v}_1,\underset{\sim}{v}_2,\Omega_L) = \frac{v_r\, v_1'\, I_{cm}(v_r,\, \theta_{cm})}{u_1^2\, |\cos\zeta|} \quad , \tag{14}$$

where (see Figure 3) $\underset{\sim}{v}_1$ and $\underset{\sim}{v}_2$ are the initial laboratory velocity vectors of the primary (detected) particle (Ar or Kr) and secondary particle (Xe), respectively, and $\Omega_L = (\Theta,\Phi)$ is the laboratory solid scattering angle with the axes shown in Figures 1 and 3. I_{cm} is the center of mass differential cross section or scattered intensity, v_r is the magnitude of the CM relative velocity, u_1 is the velocity of particle 1 in the CM frame and is

proportional to v_r, v_1' is the final laboratory velocity and ζ is the angle between the final center of mass and laboratory velocities of particle 1. We note that Eq. (14) is that appropriate for a particle density (electron impact ionization) detector. The signals for other types of detectors have other powers of v_1'. Given $\underset{\sim}{v}_1$, $\underset{\sim}{v}_2$, and Ω_L, one can easily use kinematics and geometry,[15] calculate all the velocities and angles on the rhs of Eq. (14) and, with the spline interpolation discussed above, easily generate S from I_{cm}.

However, for a real experiment, the exact calculation of the observed signal requires an 11-fold integral[16] to average S over the appropriate probability distributions for $\underset{\sim}{v}_1$, $\underset{\sim}{v}_2$, the three dimensions of the scattering center (see Fig. 1), and two angles describing the finite detector. An 11-fold numerical quadrature would be very expensive and slow. It can be performed by Monte Carlo methods, but even Monte Carlo evaluation gets expensive when one takes enough points to make the statistical error small and obtain high precision. In the present case, the properties of the molecular beam machine allow us to reduce the problem to a 4-fold integral which can be rapidly evaluated by direct quadrature.

Because (see Fig. 1) the beams are narrow and well collimated, we neglect any nonperpendicularity of the beams and the size of the scattering center in the x direction (due to the inplane width of the secondary beam), and we note that the position of a particle in the scattering center and its initial velocity direction (divergence) are correlated by the motion of the particles along streamlines. Also, the last slit shown in Figure 1 determines the solid angle subtended by the detector; the entrance slit is wide enough that the defining slit has an unobstructed view of the entire scattering center at all angles, so that no complicated detector acceptance function is needed. With these observations and approximations, we can approximate the 11-fold integral by the following 4-fold integral,

$$\overline{S}(\Phi_o) = \int_0^\infty f_1(v_1)dv_1 \int_0^\infty f_2(v_2)dv_2 \int_{-\frac{\pi}{2}}^{\pi/2} d\chi G(\chi) \int_{-\pi}^{\pi} d\Phi \; F(\Phi,\Phi_o) \; S(\underset{\sim}{v}_1,\underset{\sim}{v}_2,\Omega_L) \quad . \tag{15}$$

Here F and G are normalized effective detector functions obtained by convoluting the initial position and direction of primary particles in the scattering center with the acceptance angle of the detector defining slit. Here $\chi = \frac{\pi}{2} - \Theta$ is an out-of-plane angle, where Θ is the polar angle in the coordinate system of Figures 1 and 3, and $\sin\Theta = \cos\chi \doteq 1$ in the Jacobian. $G(\chi)$ is a trapezoid centered on zero with parameters given by Figure 4 and Table III. Symmetry of scattering about the plane allows us to actually take only positive χ in evaluating (15). F is a trapezoid centered about the experimental scattering angle Φ_o. In principle[17] its parameters should depend on Φ_o; however, the angular resolution is most important at small angles, so that the values in Table III are those appropriate for small angles. We note that without increasing the dimensionality of the quadrature one could account for all the dimensions of the scattering center leaving only 2 of the 11 dimensions (the nonperpendicularity or the divergence of the secondary beam) unaccounted for by using more complicated convolutions and Φ_o dependent effective detector functions;[17] however, that is unnecessary here.

The averaging that most affects the resolution is that over the magnitudes of the velocities of the beams. The distributions, normalized to unity when integrated over velocity, are those appropriate to nozzle beams,

$$f_i(v) = \frac{v^2}{\pi^{1/2}(\Delta v_i)[\bar{v}_i^2 + 0.5(\Delta v_i)^2]} \exp\left[-\left(\frac{v - \bar{v}_i}{\Delta v_i}\right)^2\right] \quad . \tag{16}$$

The most probable velocities, widths, and parameters of this distribution for each of the beams are given in Table III. They correspond to a most probable

relative velocity of 6.34×10^4 cm/sec (4.91×10^4 cm/sec) and a most probable relative kinetic energy of 740°K or 63.8 meV (742°K or 63.9 meV) for ArXe (KrXe).

The Φ and χ angular averages were performed using 16 and 4-point Gauss-Legendre quadrature, respectively, and the v_1 and v_2 averages used 5-point Gauss-Hermite quadrature. The resulting averaged signal is normalized to correspond to $Å^2$/sr units, and the relative experimental signal is scaled to the absolute calculated signal. The scaling factor is chosen to minimize the error discussed later.

C. Mixture Viscosities

The procedure used for calculating the viscosities, η, of the Ar-Xe and Kr-Xe mixtures has been detailed elsewhere.[18,19] Briefly, the $Q^{(n)}$ cross sections[18] were calculated at 17 relative energies between $\mathscr{E}/k_B = 50$ and 18000°K on a logarithmic spacing,[19] using quantum phase shifts at the partial waves at low energies where three turning point problems could occur and WKB phase shifts elsewhere. The maximum partial wave needed varied with energy and was found to be adequately given by $\ell_{max} = 50+10k$ ($60+12k$) for ArXe (KrXe), where k is the wavenumber in atomic units. The collision integrals $\Omega^{(n,s)}$ were then obtained using 6-point Lagrange interpolation and 8-point Gauss-Laguerre quadrature. The η_{mix} were then obtained[18] from the formulas of Monchick, Yun and Mason[20] and compared with the accurate experimental results of Kestin, Khalifa and Wakeham.[8]

D. Interaction Second Virial Coefficients

The interaction second virial coefficients, $B_{12}(T)$, were calculated classically using the usual formula.[21] Integration over r small enough that $\exp(-V/kT) < 10^{-6}$ and over r large enough to be in Region V and have $|V/kT| < 0.005$ (allowing expansion of the exponential) was performed analytically.

That over moderate r was done with two Gauss-Legendre quadratures, a 10-point quadrature for $r < r_m$ and a 32-point quadrature over $r > r_m$. The calculated $B_{12}(T)$ are compared with the experimental results of Brewer[9] and Rentschler and Schramm[10] as described in the following subsection.

E. Fitting and Uncertainties

To get a potential that will fit all three properties within experimental error it is necessary to fit the properties simultaneously. For example, if we fit the DCS alone, it is easy to find a potential which fits every oscillation in the DCS beautifully, but such a potential gives values of B and η that are far outside experimental error bounds, and that potential cannot be simply adjusted to correct B and η without destroying the DCS fit. Fits to two properties still do not fit the third. For example, one potential which fit the ArXe DCS and B gave an η which is too large by more than three times the experimental error. Fitting the three experiments simultaneously was much more of a challenge than fitting any two. To do so without trying to compare "apples and oranges," we proceeded as follows: A set of parameters was assumed and the three properties calculated at the experimental points. Then, the dimensionless mean square deviation δ_j^2 from the jth experiment was calculated from

$$\delta_j^2 = \frac{1}{n_j} \sum_{i=1}^{n_j} \Delta_{ji}^{-2} (P_{ji} - p_{ji})^2 \quad , \tag{17}$$

where P_{ji} and p_{ji} are, respectively, the calculated and experimental values of property j at point (angle or temperature)i, and Δ_{ji} is the experimental uncertainty of property j at point i. We note that with this definition, δ_j^2 and δ_j are less (greater) than unity if the average deviation

of the calculated property from experiment is less (greater) than the experimental uncertainty. Then, an overall dimensionless root mean square deviation was obtained from

$$\delta = [\frac{1}{3}\sum_{j=1}^{3} \delta_j^2]^{1/2} \quad , \tag{18}$$

and the calculations were iterated to minimize this overall δ.

To prevent improper weighting of one experiment relative to the others it is important that the uncertainties Δ_{ji} be as realistic as possible and contain an estimate of the maximum systematic error limits as well as statistical errors. Assessing these uncertainties necessitated a number of discussions (see acknowledgments) with appropriate experimentalists. For the uncertainties Δ_B we used ±2 cm^3/mole for the Brewer[9] data and ±6 cm^3/mole for the Rentschler and Schramm[10] data for both systems. For the η data[8] for both systems we used 0.4% for most of the points and 0.7% for the points at the lowest two temperatures as they appear to deviate by that amount from any smooth curve that can be drawn through the data. For the DCS data we began by using the 95% confidence limits, $\Delta_i = 2\sigma_i$, where the σ_i are the standard deviations in Tables I and II. However, these Δ_i tend to weight too heavily the small angle DCS, there the signal is very large and the relative size of σ very small. At very small angles, however, systematic errors, due to tails in the angular spread of the beams, any small nonlinearities in the detector, and any failure of Eq. (15) to describe the resolution of the machine exactly, are the largest. To account for such possible systematic errors we replaced σ_i by a geometric mean of σ_i and 5% of the signal.

Each complete iteration required less than 1 minute on a CDC 7600, so the calculation was readily repeated to convergence, using a brute force approach with manual adjustment of parameters to find the set which minimized δ. Several starting potentials were tried, and the calculations always converged to the same potential. Convergence could probably have been speeded by using a nonlinear least squares program to minimize δ, but this would need to be done carefully as the experimental properties depend on the potential parameters in a way which strongly correlates the parameters; that is, a given change in properties caused by changing one parameter can often be almost completely offset by changing another parameter. Alternatively, one could calculate the gradients or sensitivities[22] of each of the properties with respect to all the parameters and follow the path of steepest descents of δ to find the best fit. This approach would require considerable computer storage for the systems in the following paper[1] and has not yet been implemented. However, we did calculate approximate sensitivities and found them very helpful in guiding the changes to be made in the parameters as the calculations proceeded.

IV. RESULTS AND DISCUSSION

The parameters of the resulting ArXe and KrXe potentials are listed in Table IV. All are in Hartree atomic units except the x_i which are dimensionless, and the actual values used are given in the table, so that one can reproduce the potentials without roundoff errors. In this connection we have not tabulated the dependent parameters such as the β_i discussed in the text; to avoid small discontinuities they should be determined from the independent parameters and the equations in the text.

In the ArXe potential x_1 is the inflection point of V_{III} and x_1 and x_2 were not varied. In the KrXe potential x_2 was not varied. The van der Waals C_8 and C_{10} coefficients are the mean (upper bound) values of Tang, et al.[23] for ArXe (KrXe) and were not varied to any extent. However, the C_6 coefficients (Table IV) required to fit the data are significantly larger than the values of 129±5 (184±9) recommended in Ref. 23. When this was first observed, it was thought that the larger C_6's were being required due to the potential form used and were compensating for some defect in the shape of the potential in the spline region. However, after completing this work, we learned that there is evidence [24] that the Tang, et al.[23] values of C_6 for Xe systems are too small, and the most recent determination[25] of the ArXe C_6 gave value (140.3±1.2) almost as large as that required here.

The uncertainties shown in Table IV are the changes in each parameter that will raise the overall deviation δ by 0.02. Any change of a single parameter by more than the uncertainty shown will result in a significantly worse fit to one or more of the three properties used here. However, if one were to fit additional data simultaneously with these properties, changes of these parameters by several times the uncertainty shown are probably possible if several parameters are changed in largely compensating ways. In particular, the uncertainty in α_I is large because none of the data available is sensitive to the repulsive wall of the potential at energies above about 1000 K.

The dimensionless rms deviations δ_i of each property and the overall rms deviation δ are shown in Table V. One sees there that the fits are very good, well within the experimental uncertainties of all three properties.

The laboratory differential cross sections from the present experiments and the calculated laboratory cross sections, after transformation and averaging, are compared in Figures 5 and 6. The full experimental uncertainty Δ used in the fitting is also shown for a few representative points. The fits are very good. For ArXe the calculated result is well within experimental error everywhere except in the vicinity of the primary rainbow minimum. For KrXe the error is noticeable throughout the region of the primary rainbow maximum and minimum. These errors could easily be removed but not without a deterioration of the fit to the other properties. This primary rainbow region of the DCS is very sensitive to the detailed shape of the potential in the spline region, and, in our opinion, these errors are due to some small but fundamental weakness of the MSV potential form. To correct them while keeping the DCS accurate at all smaller angles and also keeping a good fit to η and B will require a nontrivial improvement in the form of the potential.

Mixture viscosities in micropoise (1 Poise = 1g cm^{-1} sec^{-1}) for the mixtures of Kestin et. al[8] that are most sensitive to the unlike interactions of present interest are plotted versus temperature in Figures 7 and 8. The experimental uncertainties are just slightly larger than the heavy points shown, and one sees that the fit is excellent.

The calculated interaction second virial coefficients are compared with the experimental values[9,10] in Figures 9 and 10. Again, the fit is excellent.

To see how well these potentials can predict a property not included in the fitting procedure, we have calculated the diffusion coefficients, and

these are compared with experiment[26-29] in Figures 11 and 12. The agreement is very good, as expected, because viscosity data were used in determining the potentials, and diffusion is sensitive to the same features of the potential as viscosity. Although the calculated points for KrXe at the highest temperatures lie outside the published error estimates of Ref. 29, we do not think any adjustment of the potential is warranted because the effect is already visible by 800°K where our calculated results agree with the accurate viscosity data of Ref. 8 and also with the D of Ref. 28. Not shown on the plot is the accurate ArXe D of Arora, Robjohns and Dunlop[30] of 0.1140 cm^2/sec at 300°K, believed accurate to within 0.2%. Our calculated value, 0.1144 cm^2/sec, is only 0.3% high, but the calculated D and η are both slightly larger than experiment at this temperature, so that, if one wished, he could make a slight improvement to the ArXe potential by requiring that, in addition to the properties already used, this D measurement also be fit.

For the use of the reader, the calculated collision integrals[18] $\Omega(n,s)$ for the two systems are reproduced in Tables VI and VII.

Before concluding this section let us consider the sources of error in the present potentials and ways in which they may be improved. First, although the M3SV potentials are flexible, some dependence on the form of the potential is still undoubtedly present, and more realistic forms would improve the potential. Second, although we have tried to check the convergence of all numerical procedures carefully, there may still be small errors due to roundoff, etc., and our use of WKB phase shifts can introduce small errors, usually only a few tenths of a percent at most, in the calculated cross sections. In addition, the velocity and angular spreads of real molecular beams are never really quite as simple as the models used; however, because (see Figs. 5 and 6) our <u>a priori</u> calculated resolution of the rainbow oscillations

of the differential cross section agrees well with experiment--the calculated resolution is slightly poorer (better) for ArXe (KrXe) than the experimental resolution--we expect that improvements in the modeling of the beam machine will have only very small effects. Calculation of quantum corrections[31] to the classical virial coefficients used herein would increase B slightly at the lowest temperatures considered and perhaps require C_6 to be a bit larger even than we obtained here. And of course if any of the experimental data used in the fitting are really in error by more than the error limits used, the resulting potentials will be correspondingly in error. Also, since the repulsive walls of the present potentials may be very inaccurate at energies above about 1000 K (0.003 a.u.), if new data sensitive to the higher energy part of the potential were to become available, it could be used to improve these potentials.

At present, we are aware of two recent experiments that provide data accurate enough to be used to improve these potentials. One is the diffusion coefficient datum[30] already mentioned. The other experiment is the recent measurement of the integral cross section by van den Biesen, et. al.[4] These latter data were not included in the present calculations because we only became aware of them as this work was nearing completion, only plots without tables are given in the papers, and because similar data is not available on the systems[1] $ArSF_6$ and $KrSF_6$ for which this work is a prototype. Because the $\varepsilon = 5.93 \times 10^{-4} (7.32 \times 10^{-4})$ and $r_m = 7.67$ (7.90) a.u. obtained for ArXe (KrXe) by van den Biesen, et. al[4], are almost the same as those obtained here, we expect any change required in these potentials due to inclusion of the integral cross section data to be very small. However, that data, like the DCS, is sensitive to the attractive part of the potential, and it would be an interesting test of the spline portion of these potentials to see how well they reproduce those results.

V. CONCLUSION

In this paper we have reported high quality differential scattering cross sections for the ArXe and KrXe systems. Using these data and complementary viscosity and virial coefficient data, we have determined interatomic potentials that simultaneously fit all three properties within experimental error. The resulting potentials were tested against diffusion data and found to predict it very well. These are the first Class I multiproperty potentials to be determined for these two systems.

ACKNOWLEDGMENTS

We would like to thank Profs. B. Schramm and J. Kestin for helpful discussions. One of us (RTP) wishes to thank the Max Planck Institut für Strömungsforschung, Göttingen, West Germany, for its hospitality and the Alexander von Humboldt Foundation for a senior U. S. Scientist Award under which part of this work was done. He also thanks Dr. M. Fäubel, Prof. U. Buck, and Prof. J. P. Toennies for many helpful discussions.

This work was supported by the Director, Office of Energy Research, Office of Basic Energy Sciences, Chemical Sciences Division of the U.S. Department of Energy under Contract DE-AC03-76SF00098.

REFERENCES

1. R. T Pack, J. J. Valentini, and J. B. Cross, J. Chem. Phys. 77, 0000 (1982), following paper.

2. J. M. Parson, T. P. Shafer, P. E. Siska, F. P. Tully, Y. C. Wong, and Y. T. Lee, J. Chem. Phys. 53, 3755 (1970).

3. M. V. Bobetic and J. A. Barker, J. Chem. Phys. 64, 2367 (1976).

4. J.J.H. van den Biesen, F. A. Stokvis, E. H. van Veen, and C.J.N. van den Meijdenberg, Physica 100A, 375 (1980) and references therein.

5. G. C. Maitland and W. A. Wakeham, Mol. Phys. 35, 1443 (1978).

6. J. K. Lee, D. Henderson, and J. A. Barker, Mol. Phys. 29, 429 (1974).

7. G. C. Maitland, M. Rigby, E. B. Smith, and W. A. Wakeham, Intermolecular Forces: Their Origin and Determination (Oxford U. Press, Oxford, England, 1980) p. 506.

8. J. Kestin, H. E. Khalifa and W. A. Wakeham, Physica 90A, 215 (1978).

9. J. Brewer, Tech. Rept AD663448, AFOSR Contract No. AF49(638)-1620 (1967). Available from the Clearinghouse for Federal Scientific and Technical Information.

10. H. P. Rentschler and B. Schramm, Ber. Bunsenges Phys. Chem. 81, 319 (1977).

11. See for example, P. E. Siska, J. M. Parson, J. P. Schafer, and Y. T. Lee, J. Chem. Phys. 55, 5762 (1971).

12. R. Düren and Ch. Schlier, Disc. Faraday Soc. 40, 56 (1965).

13. See, for example, N. F. Mott and H.S.W. Massey, The Theory of Atomic Collisions, 3rd ed. (Oxford U. Press, London, 1965) pp.20-24.

14. R. T Pack, J. Chem. Phys. 60, 633 (1974).

15. See, for example, T. T. Warnock and R. B. Bernstein, J. Chem. Phys. 49, 1878 (1968) and 51, 4682 (1969).

16. See, for example, M. Faubel and J. P. Toennies, Adv. At. Mol. Phys. 13, 229 (1978).

17. R. T Pack, unpublished work.

18. G. A. Parker and R. T Pack, J. Chem. Phys. 68, 1585 (1978).

19. R. T Pack, J. Chem. Phys. 70, 3424 (1979).

20. L. Monchick, K. S. Yun, and E. A. Mason, J. Chem. Phys. 39, 654 (1963).

21. See, for example, J. H. Dymond and E. B. Smith, The Virial Coefficients of Pure Gases and Mixtures (Oxford U. Press, London, 1980).

22. See, for example, L. Eno and H. Rabitz, J. Chem. Phys. 74, 3859 (1981).

23. K. T. Tang, J. M. Norbeck, and P. R. Certain, J. Chem. Phys. 64, 3063 (1976).

24. K. T. Tang, private communication; K. T. Tang and J. P. Toennies, J. Chem. Phys. 74, 1148 (1981).

25. H.C.W. Beijerinck, P.M.A. van der Kam, E.J.E. Cottaar, and N. F. Verster, J. Chem. Phys. 75, 1570 (1981).

26. W. Hogervorst, Physica 51, 59 (1971).

27. R.J.J. van Heijningen, J. P. Harpe, and J.J.M. Beenakker, Physica 38, 1 (1968).

28. A. E. Loiko, B. A. Ivakin, and P. E. Suetin, Zh. Tekh. Fiz. 44, 682 (1974)[English translation: Sov. Phys. Tech. Phys. 19, 434 (1974)].

29. D. Cain and W. L. Taylor, J. Chem. Phys. 71, 3601 (1979).

30. P. S. Arora, H. L. Robjohns, and P. J. Dunlop, Physica 95A, 561 (1979).

31. J. O. Hirschfelder, C. F. Curtiss, and R. B. Bird, Molecular Theory of Gases and Liquids (Wiley, N.Y., 1954) p. 420.

Table I. Experimental LAB scattering angle Φ_o, signal S, and standard deviation σ for ArXe.

Φ_o	S	σ	Φ_o	S	σ
3.4	7.295	0.054	15.9	0.328	0.006
3.65	6.355	0.095	16.4	0.343	0.006
3.9	5.447	0.086	16.9	0.352	0.003
4.15	4.633	0.050	17.4	0.356	0.003
4.4	3.948	0.041	17.9	0.351	0.003
4.65	3.282	0.073	18.4	0.340	0.001
4.9	2.650	0.069	18.9	0.324	0.002
5.15	2.187	0.020	19.4	0.307	0.003
5.4	1.840	0.011	19.9	0.284	0.004
5.65	1.552	0.020	20.4	0.262	0.003
5.9	1.331	0.049	20.9	0.241	0.002
6.15	1.189	0.038	21.4	0.219	0.002
6.4	1.115	0.032	21.9	0.198	0.001
6.9	1.071	0.044	22.4	0.178	0.001
7.4	1.077	0.041	23.4	0.142	0.001
7.9	1.083	0.028	24.4	0.113	0.001
8.4	1.062	0.036	25.4	0.090	0.001
8.9	1.000	0.010	26.4	0.075	0.001
9.4	0.901	0.010	27.4	0.061	0.001
9.9	0.769	0.009	28.4	0.054	0.001
10.4	0.631	0.018	29.4	0.047	0.001
10.9	0.495	0.014	30.4	0.043	0.001
11.4	0.393	0.015	32.4	0.037	0.001
11.9	0.308	0.007	34.4	0.033	0.001
12.4	0.255	0.003	36.4	0.031	0.001
12.9	0.226	0.003	38.4	0.030	0.001
13.4	0.224	0.004	40.4	0.028	0.001
13.9	0.233	0.006	42.4	0.027	0.001
14.4	0.252	0.007	44.4	0.027	0.001
14.9	0.282	0.007	46.4	0.028	0.002
15.4	0.307	0.010	48.4	0.026	0.001
			50.4	0.024	0.001

Table II. Experimental LAB scattering angle Φ_o, signal S, and standard deviation σ for KrXe.

Φ_o	S	σ	Φ_o	S	σ
3.40	11.366	0.049	16.9	0.457	0.012
3.65	9.711	0.074	17.4	0.495	0.007
3.90	8.716	0.098	17.9	0.532	0.004
4.15	7.859	0.049	18.4	0.559	0.004
4.40	7.302	0.040	18.9	0.587	0.005
4.65	6.792	0.056	19.4	0.594	0.006
4.90	6.120	0.081	19.9	0.593	0.007
5.15	5.400	0.059	20.4	0.580	0.005
5.40	4.613	0.030	20.9	0.559	0.004
5.65	4.043	0.020	21.4	0.525	0.005
5.90	3.435	0.021	21.9	0.486	0.004
6.15	3.025	0.036	22.4	0.460	0.004
6.40	2.699	0.028	23.4	0.372	0.004
6.90	2.459	0.013	24.4	0.303	0.006
7.40	2.366	0.021	25.4	0.245	0.005
7.90	2.263	0.012	26.4	0.200	0.003
8.40	1.978	0.006	27.4	0.167	0.006
8.90	1.651	0.011	28.4	0.148	0.005
9.40	1.303	0.025	29.4	0.133	0.009
9.90	1.080	0.017	30.4	0.114	0.005
10.4	0.971	0.004	32.4	0.099	0.003
10.9	0.949	0.004	34.4	0.089	0.006
11.4	0.989	0.014	36.4	0.087	0.005
11.9	1.018	0.013	38.4	0.081	0.003
12.4	1.000	0.010	40.4	0.075	0.003
12.9	0.946	0.011	42.4	0.077	0.008
13.4	0.854	0.004	44.4	0.071	0.005
13.9	0.737	0.003	46.4	0.068	0.003
14.4	0.626	0.004	48.4	0.069	0.003
14.9	0.534	0.006	50.4	0.067	0.003
15.4	0.466	0.010	52.4	0.068	0.003
15.9	0.440	0.005	54.4	0.064	0.003
16.4	0.441	0.005	56.4	0.061	0.003

Table III. Parameters used in describing the resolution of the molecular beam machine used in the DCS measurements. See the text for details.

Parameters	Beam		
	Ar	Kr	Xe
A_Φ (inplane)	0.63°	0.63°	
B_Φ (inplane)	0.55°	0.55°	
A_χ (out of plane)	1.03°	1.03°	
B_χ (out of plane)	0.63°	0.63°	
v_{prob} (cm/sec)	5.55×10^4	3.83×10^4	3.07×10^4
FWHM ($\%v_{prob}$)	13.8	13.0	12.0
$\bar{v}$ (cm/sec)	5.51×10^4	3.81×10^4	3.05×10^4
Δv	0.46×10^4	0.30×10^4	0.22×10^4

Table IV. Potential parameters in Hartree atomic units.

Parameter	ArXe	KrXe
ε	$(5.98\pm.02)\times10^{-4}$	$(7.33\pm.02)\times10^{-4}$
r_m	7.63±.01	7.92±.01
α_I	1.03±.09	0.81±.09
α_{II}	0.884±.009	0.810±.007
α_{III}	0.820±.008	0.772±.008
$x_1 = r_1/r_m$	infl. pt.	1.16±.02
$x_2 = r_2/r_m$	1.45	1.40
C_6	147±3.	210.±8.
C_8	3170.	5787.
C_{10}	93400.	179500.

Table V. Comparison of calculated and experimental properties. Dimensionless rms deviations of virial coefficients (B), viscosities (η), and differential cross sections (DCS), and the overall dimensionless rms deviation. See the text for details.

Deviation	ArXe	KrXe
δ_B	0.26	0.48
δ_η	0.56	0.63
δ_{DCS}	0.54	0.84
δ	0.47	0.67

Table VI. ArXe collision integrals $\Omega^{(n,s)}$ in units of cm^3/sec.

T(K)	$\Omega^{(1,1)}$	$\Omega^{(1,2)}$	$\Omega^{(1,3)}$	$\Omega^{(2,1)}$	$\Omega^{(2,2)}$	$\Omega^{(2,3)}$
150	.51534-10	.13054-09	.46390-09	.44739-10	.11495-09	.40387-09
200	.52126-10	.13330-09	.48236-09	.45408-10	.11561-09	.40894-09
300	.54551-10	.14292-09	.52838-09	.46506-10	.11875-09	.42897-09
400	.56700-10	.15252-09	.57234-09	.47824-10	.12415-09	.45607-09
500	.59136-10	.16177-09	.61236-09	.49110-10	.12990-09	.48341-09
600	.61824-10	.17071-09	.64926-09	.50414-10	.13571-09	.51002-09
700	.64398-10	.17896-09	.68278-09	.51847-10	.14138-09	.53495-09
800	.66917-10	.18678-09	.71394-09	.53453-10	.14704-09	.55883-09
900	.69326-10	.19408-09	.74285-09	.55052-10	.15242-09	.58128-09
1000	.71586-10	.20090-09	.76976-09	.56619-10	.15756-09	.60241-09
1100	.73750-10	.20737-09	.79507-09	.58176-10	.16252-09	.62250-09
1200	.75833-10	.21352-09	.81900-09	.59722-10	.16732-09	.64168-09

Table VII. KrXe collision integrals $\Omega^{(n,s)}$ in units of cm^3/sec.

T(K)	$\Omega^{(1,1)}$	$\Omega^{(1,2)}$	$\Omega^{(1,3)}$	$\Omega^{(2,1)}$	$\Omega^{(2,2)}$	$\Omega^{(2,3)}$
150	.46798-10	.11829-09	.41494-09	.40337-10	.10446-09	.36854-09
200	.46766-10	.11868-09	.42300-09	.41436-10	.10594-09	.37160-09
300	.48386-10	.12404-09	.45103-09	.41439-10	.10610-09	.37930-09
400	.49677-10	.13039-09	.48167-09	.42748-10	.10939-09	.39598-09
500	.51120-10	.13670-09	.51037-09	.43790-10	.11330-09	.41487-09
600	.52770-10	.14295-09	.53726-09	.44554-10	.11722-09	.43400-09
700	.54451-10	.14882-09	.56176-09	.45438-10	.12116-09	.45225-09
800	.56203-10	.15451-09	.58470-09	.46471-10	.12523-09	.47008-09
900	.57912-10	.15983-09	.60596-09	.47487-10	.12910-09	.48690-09
1000	.59526-10	.16481-09	.62569-09	.48537-10	.13286-009	.50280-09
1100	.61094-10	.16954-09	.64420-09	.49622-10	.13654-09	.51799-09
1200	.62624-10	.17406-09	.66170-09	.50724-10	.14013-09	.53253-09

FIGURE CAPTIONS

1. Schematic showing the geometry of the molecular beam machine used in the DCS measurements. The primary beam collimating slit is 0.029" wide (in-plane) and 0.055" high (out of plane). The secondary beam collimating slit is a 0.067" diameter skimmer. All detector openings are 0.121" square. The geometric full width dimensions of the scattering center are (x,y,z) = (0.098", 0.039", 0.073"). The skimmers are ~0.03" in diameter and ~0.25" from the nozzles.

2. Typical M3SV potential with regions to scale. Regions I, II, and III are the Morse potential regions; IV is the spline region, and V is the long range van der Waals region.

3. Newton diagram showing relations between center of mass and laboratory quantities. $\underset{\sim}{v}_1$ and $\underset{\sim}{v}_2$ are initial lab velocities; $\underset{\sim}{v}_1'$ is the final lab velocity of the primary (detected) particle. $\underset{\sim}{v}_{cm}$ and $\underset{\sim}{v}_r$ are the center of mass and relative velocities. $\underset{\sim}{u}_1$ and $\underset{\sim}{u}_1'$ are the initial and final velocities of the primary particle in the c.m. frame. Θ_{cm} and Φ are the center of mass and lab scattering angles, respectively, and ζ is the angle beteeen the final cm and lab velocities of the primary particle. The possible divergences of $\underset{\sim}{v}_1$ and $\underset{\sim}{v}_2$ from the axes are exagerated for clarity.

4. Trapezoid parameters used for effective detector height and width. The full width at half maximum is 2A, and each sloping region (penumbra) is of length 2B.

5. ArXe laboratory differential scattering versus laboratory scattering angle in degrees. The solid line is the calculated result, the points are from the present experiment. Uncertainties of a few representative points are shown. The arbitrary units here are chosen to correspond to square Angstroms per steradian.

6. KrXe laboratory differential scattering. The notation is the same as Figure 5.

7. ArXe mixture viscosity in micropoise (1 Poise = 1g cm^{-1} sec^{-1}) versus temperature in Kelvin for a mixture sensitive to the ArXe interaction. The solid line is calculated; the heavy points are from the experiments of Ref. 8. The experimental uncertainty is slightly larger than the size of the heavy points.

8. KrXe mixture viscosity versus temperature. The notation is that of Fig. 7.

9. ArXe interaction second virial coefficients in cm^3/mole versus temperature in Kelvin. The solid line is calculated; the experimental points are from Refs. 9 and 10.

10. KrXe interaction second virial coefficients. The notation is that of Figure 9.

11. ArXe diffusion coefficients in cm^2/sec versus absolute temperature. The solid line is calculated; the experimental points are from Refs. 26-28.

12. KrXe diffusion coefficients in cm^2/sec versus absolute temperature. The solid line is calculated: the experimental points are from Refs. 27-29.

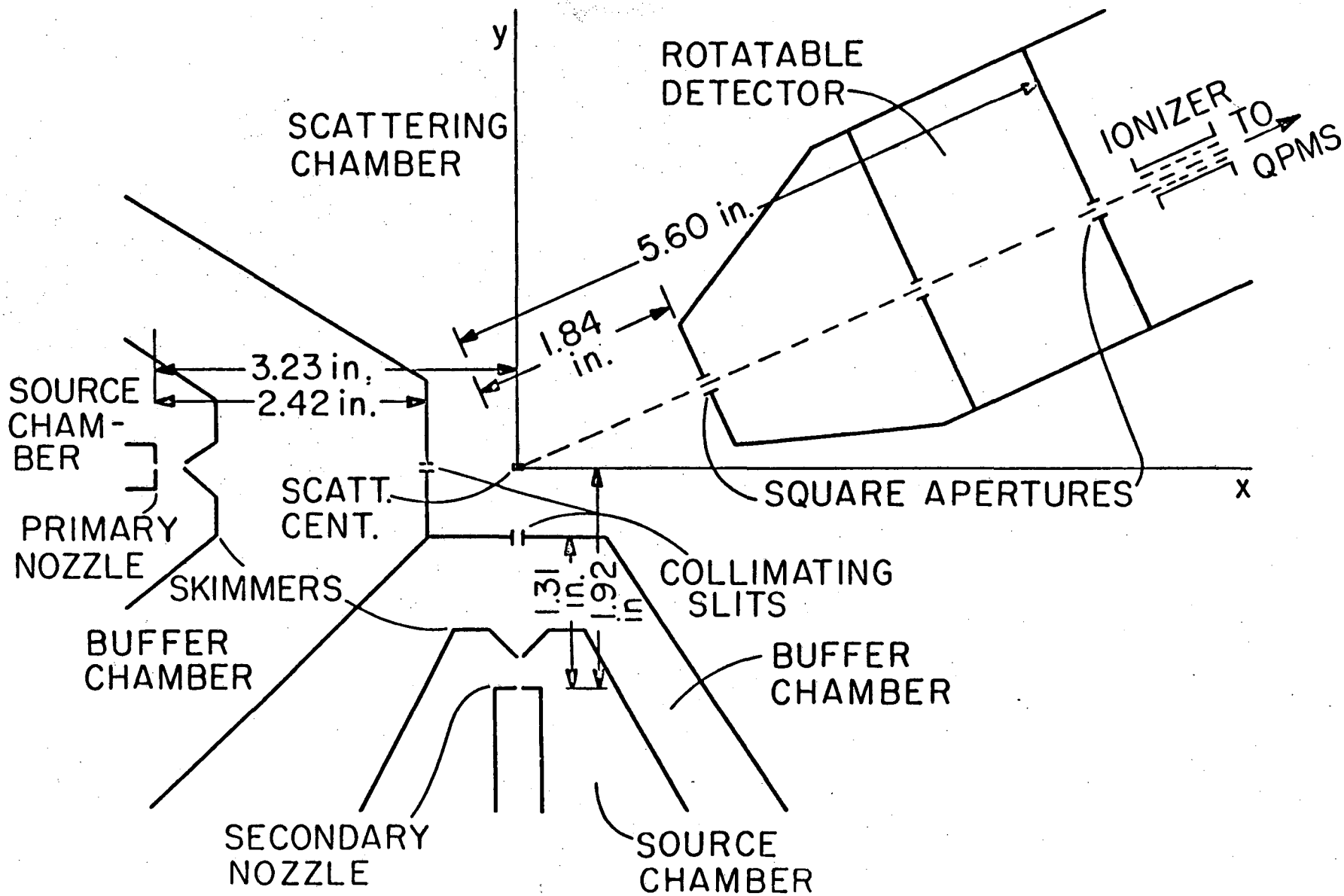
y
SCATTERING CHAMBER
ROTATABLE DETECTOR
IONIZER
TO QPMS
5.60 in.
1.84 in.
3.23 in.
2.42 in.
SOURCE CHAM-BER
PRIMARY NOZZLE
SCATT. CENT.
SQUARE APERTURES
x
COLLIMATING SLITS
SKIMMERS
.31 in.
.92 in.
BUFFER CHAMBER
BUFFER CHAMBER
SECONDARY NOZZLE
SOURCE CHAMBER

Fig. 1.

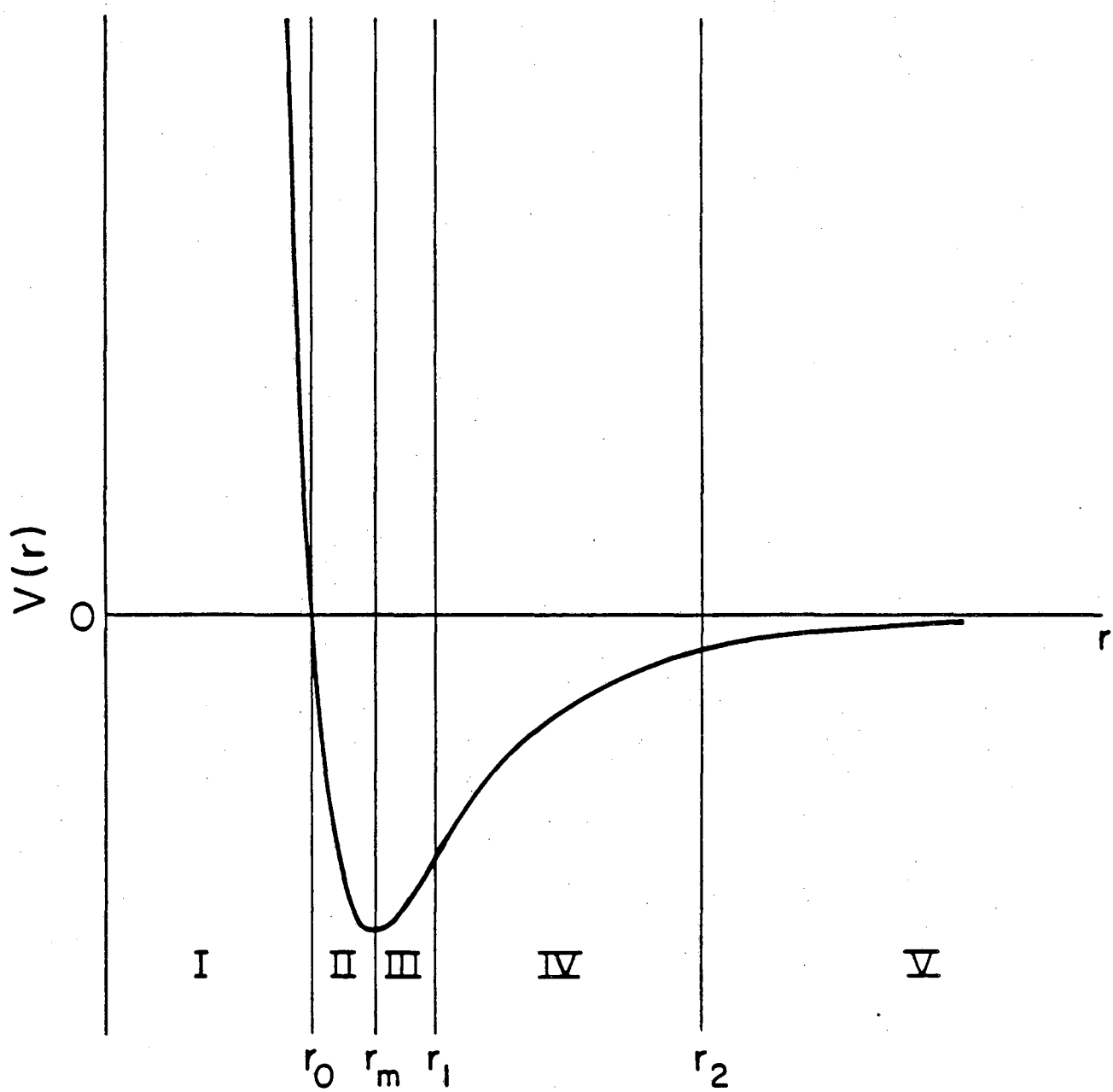

Fig. 2.

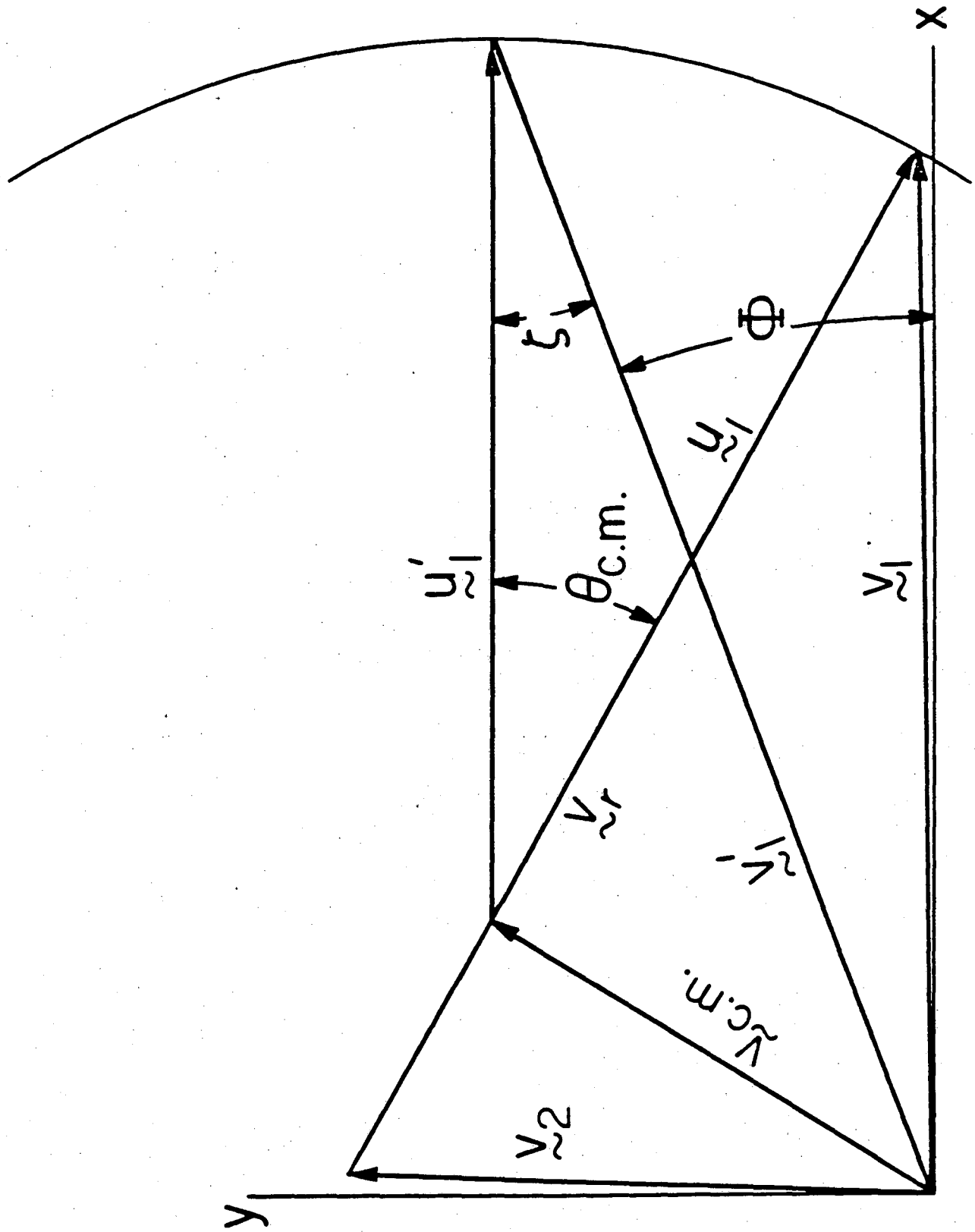
x
y
ζ
Φ
$\underset{\sim}{u}_1$
$\underset{\sim}{u}_1'$
$\theta_{c.m.}$
$\underset{\sim}{v}_1$
$\underset{\sim}{v}_r$
$\underset{\sim}{v}_1'$
$\underset{\sim}{v}_{c.m.}$
$\underset{\sim}{v}_2$

Fig. 3.

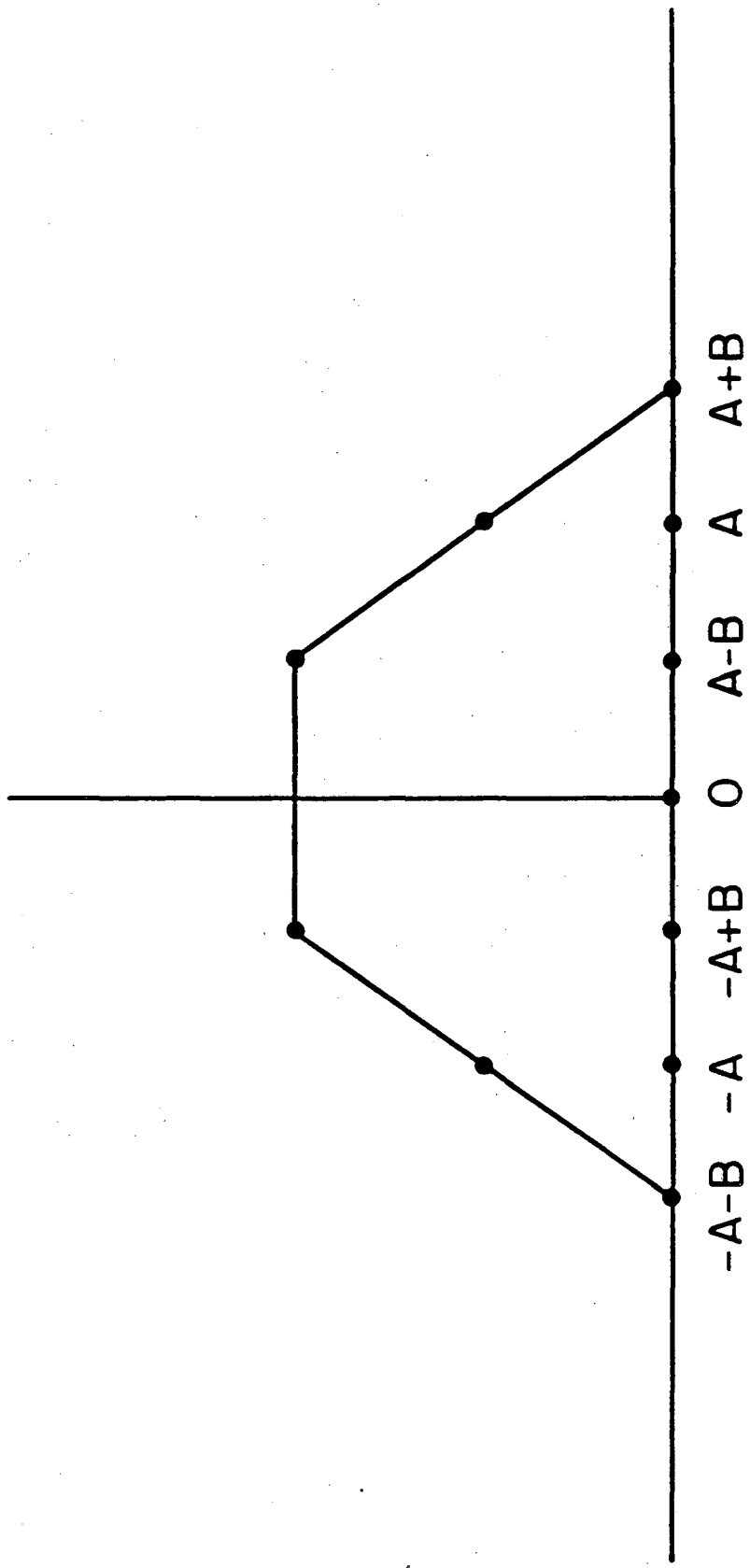

Fig. 4.

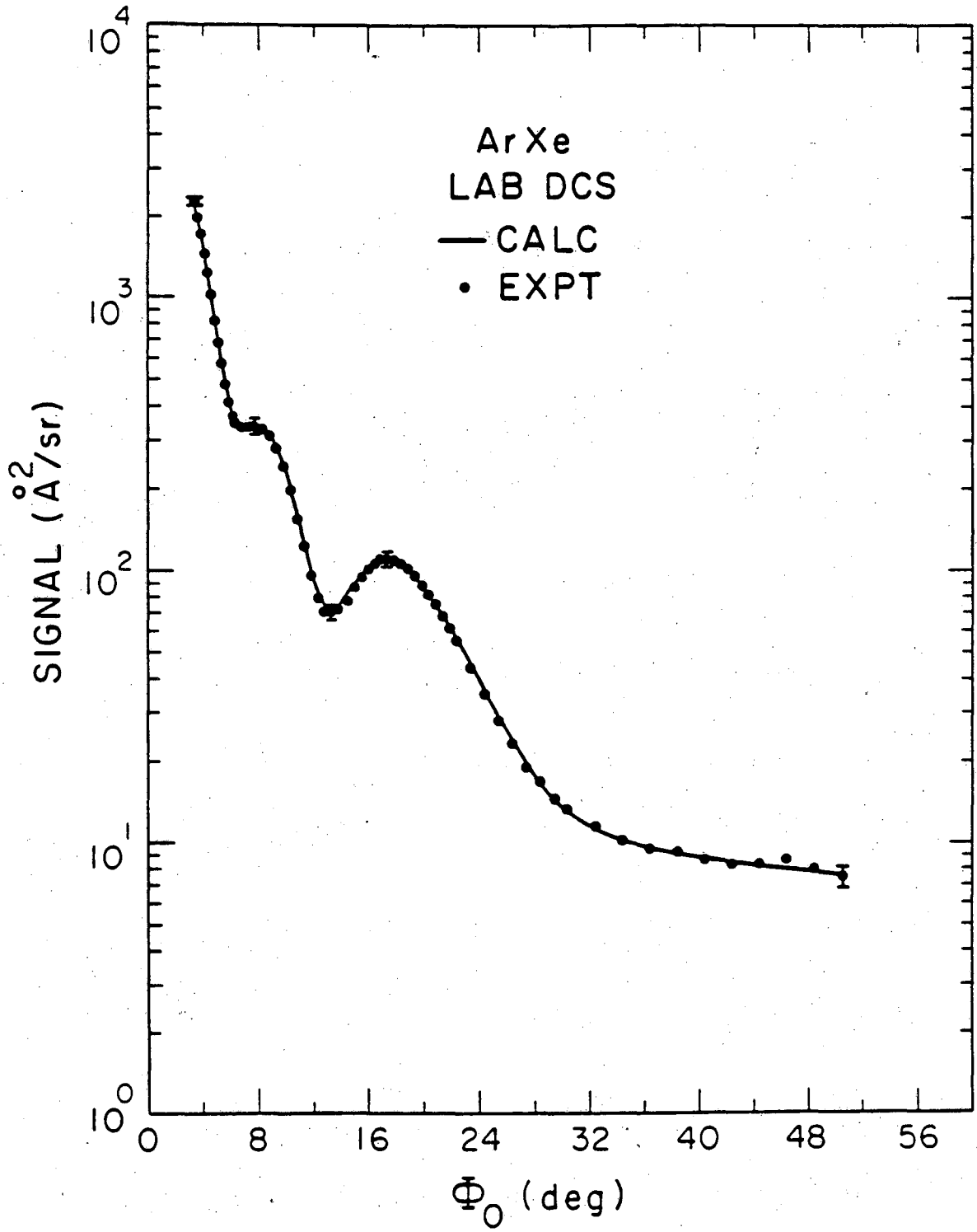
ArXe
LAB DCS
CALC
EXPT
SIGNAL (Å²/sr)
10⁴
10³
10²
10¹
10⁰
0
8
16
24
32
40
48
56
Φ0 (deg)

Fig. 5.

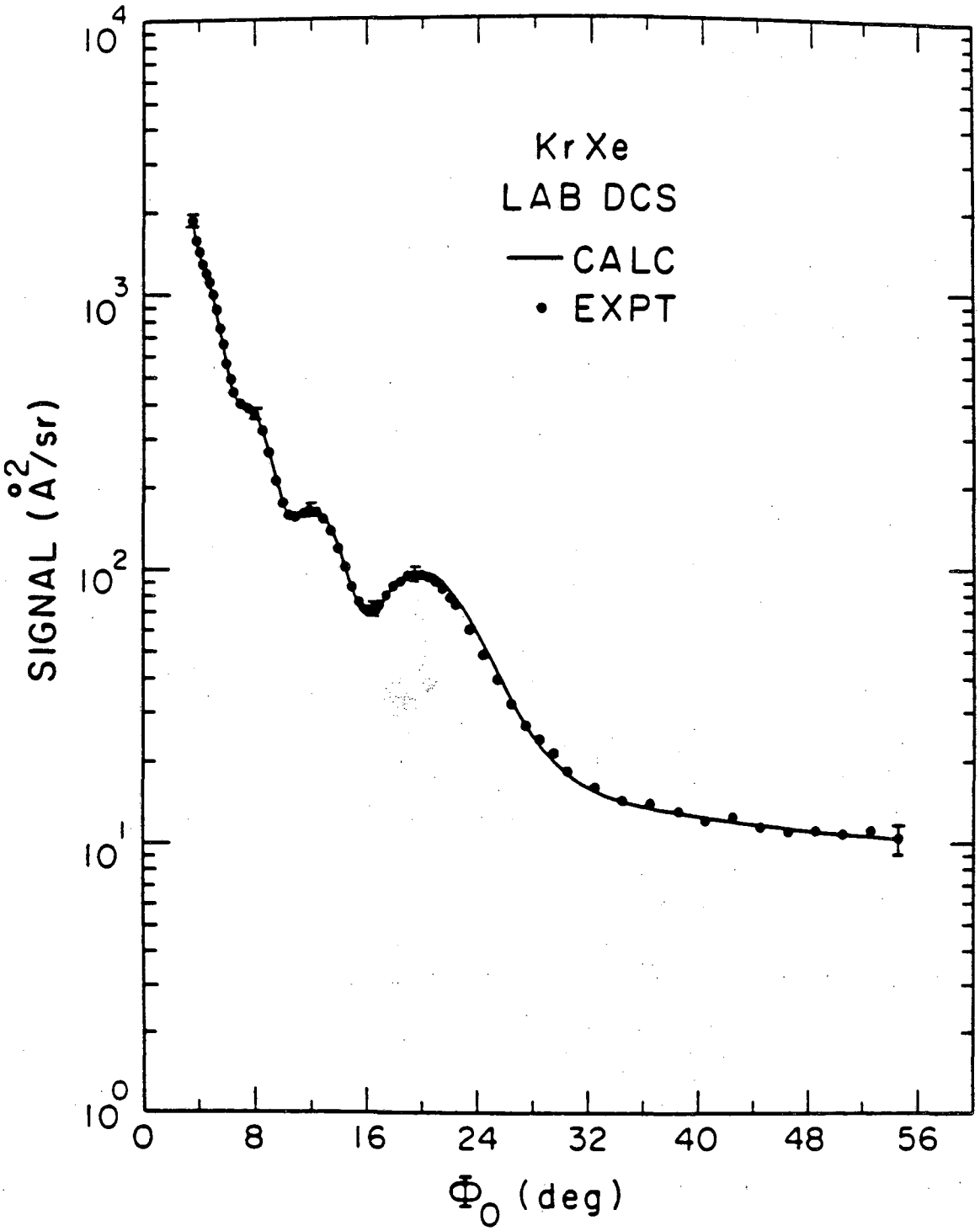
KrXe
LAB DCS
CALC
EXPT
SIGNAL (Å²/sr)
10⁴
10³
10²
10¹
10⁰
0
8
16
24
32
40
48
56
Φ0 (deg)

Fig. 6.

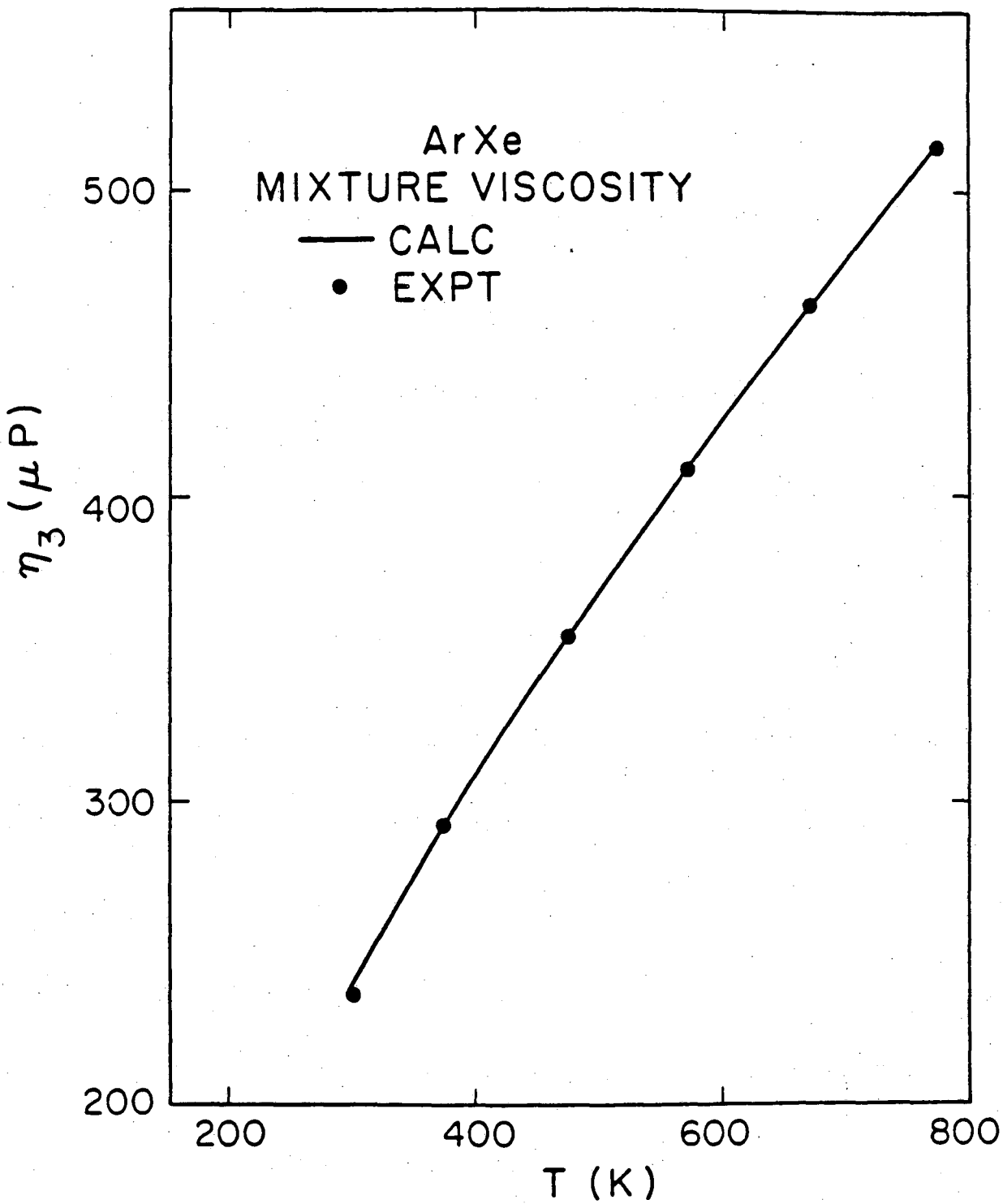
ArXe
MIXTURE VISCOSITY
CALC
EXPT
500
400
300
200
η_3 (μP)
200
400
600
800
T (K)

Fig. 7.

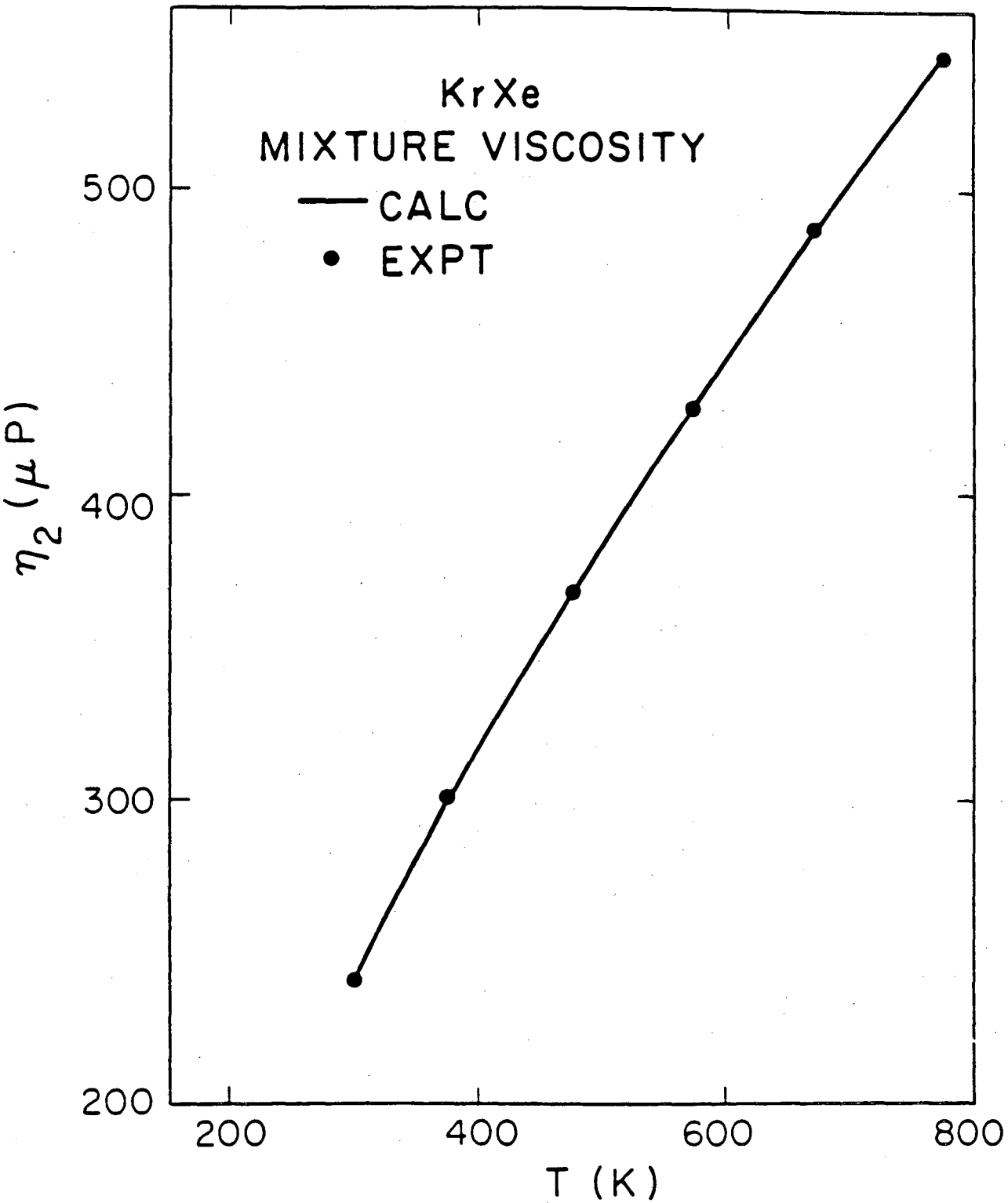
KrXe
MIXTURE VISCOSITY
CALC
EXPT
500
400
300
200
η_2 (μP)
200
400
600
800
T (K)

Fig. 8.

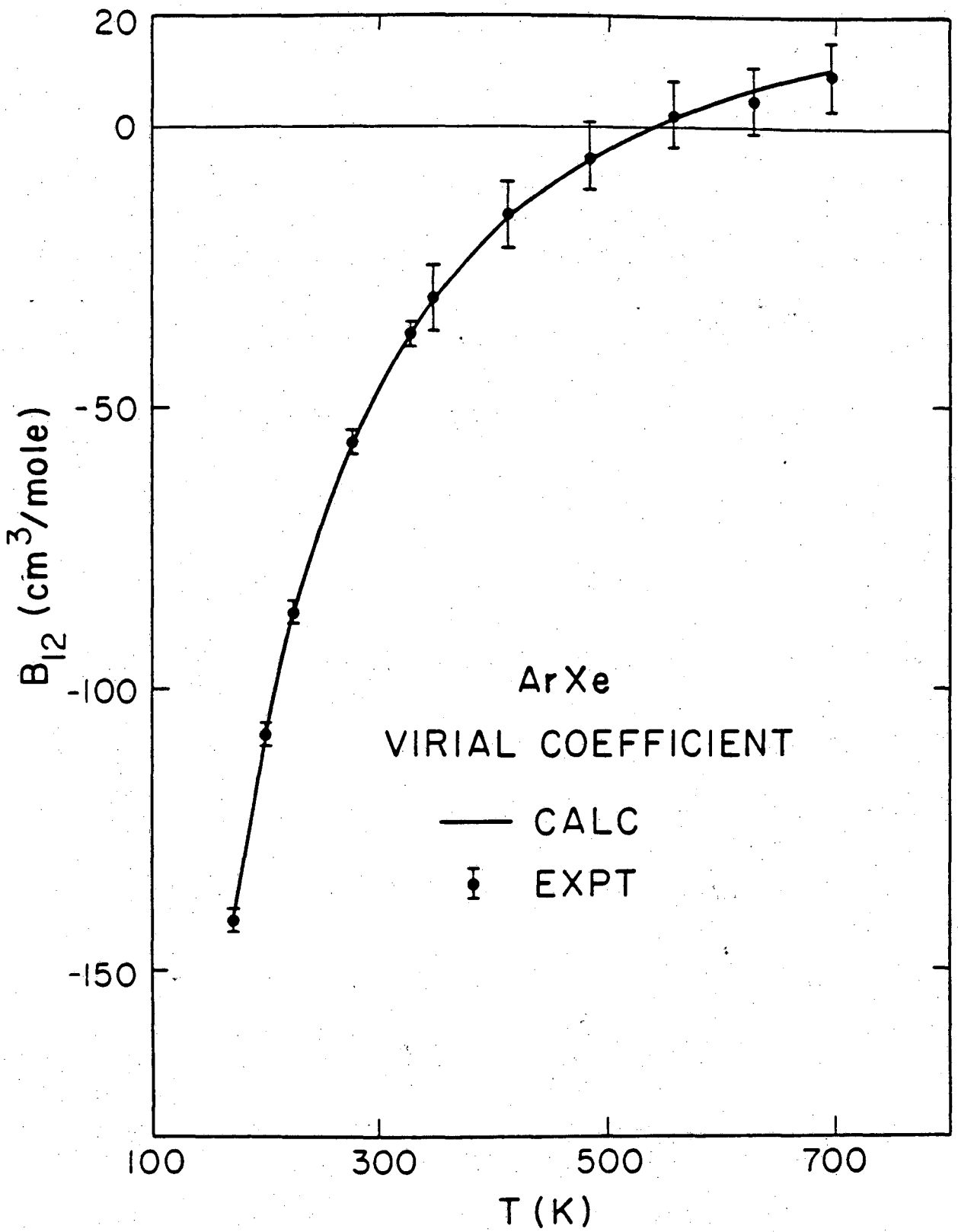
20
0
-50
-100
-150
B_{12} (cm^3/mole)
ArXe
VIRIAL COEFFICIENT
CALC
EXPT
100
300
500
700
T (K)

Fig. 9.

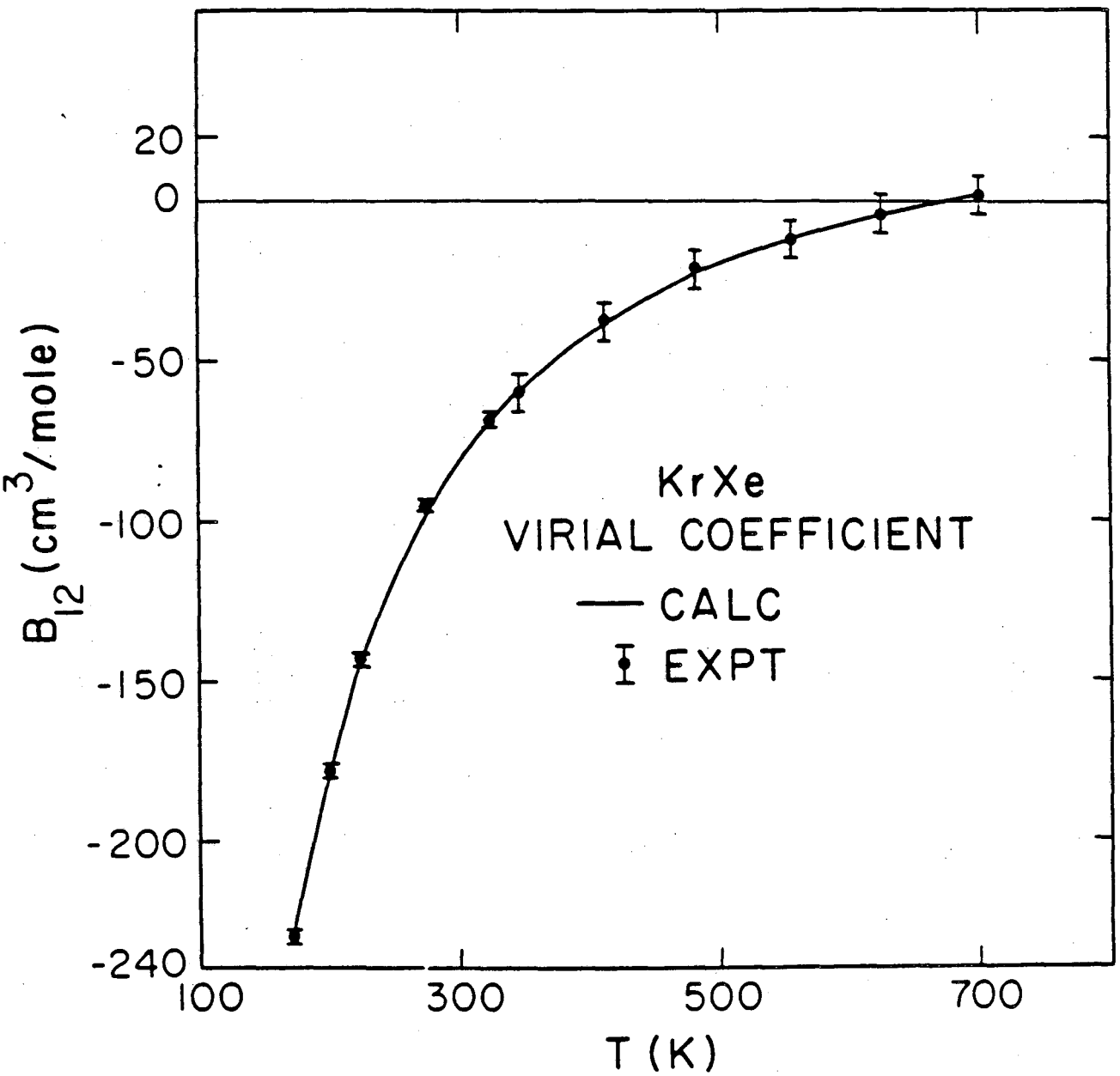
20
0
-50
-100
-150
-200
-240
100
300
500
700
T (K)
B_{12} (cm^3/mole)
KrXe
VIRIAL COEFFICIENT
CALC
EXPT

Fig. 10.

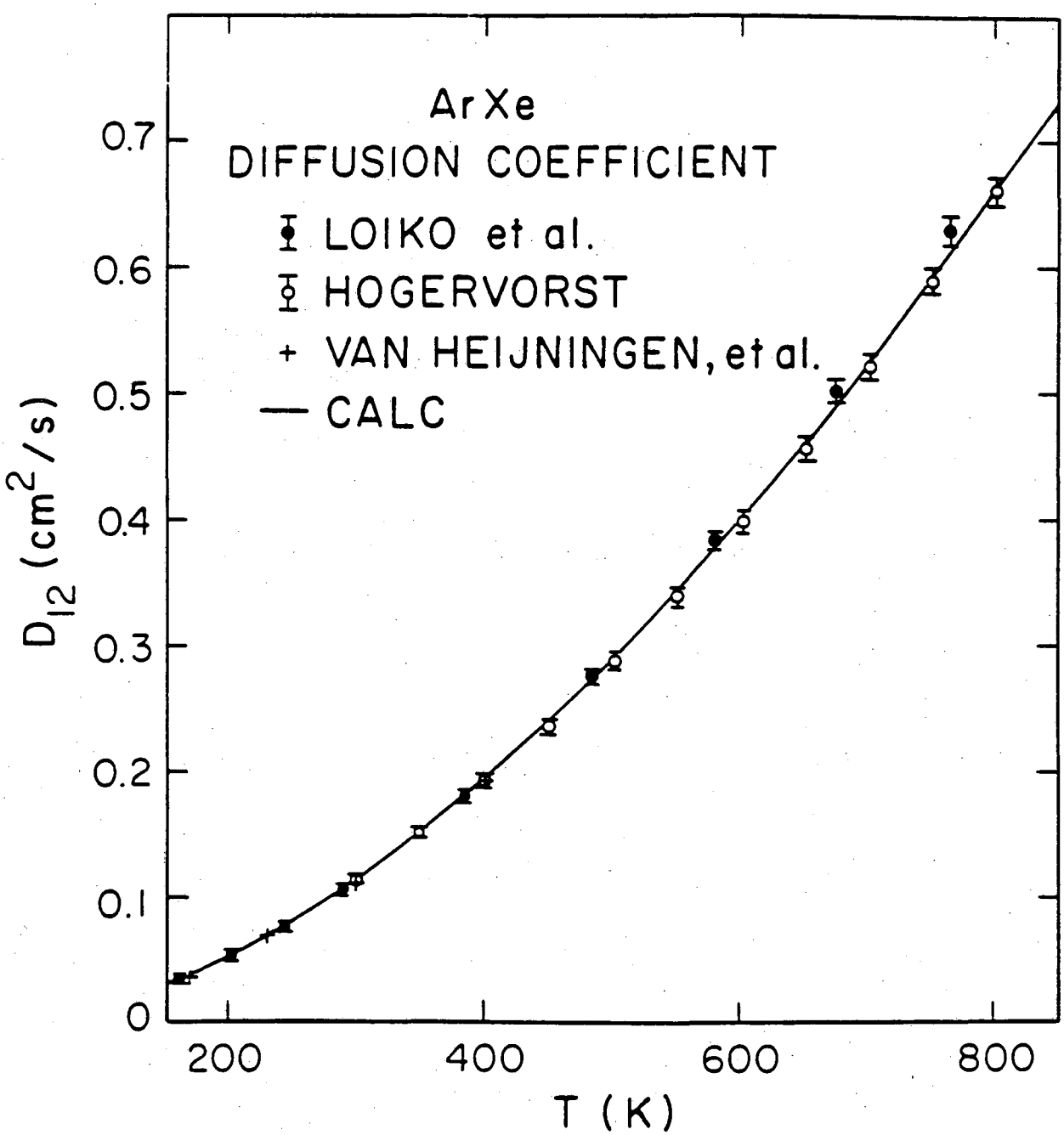
Ar Xe
DIFFUSION COEFFICIENT
LOIKO et al.
HOGERVORST
+ VAN HEIJNINGEN, et al.
— CALC
0.7
0.6
0.5
0.4
0.3
0.2
0.1
0
D_{12} (cm^2/s)
200
400
600
800
T (K)

Fig. 11.

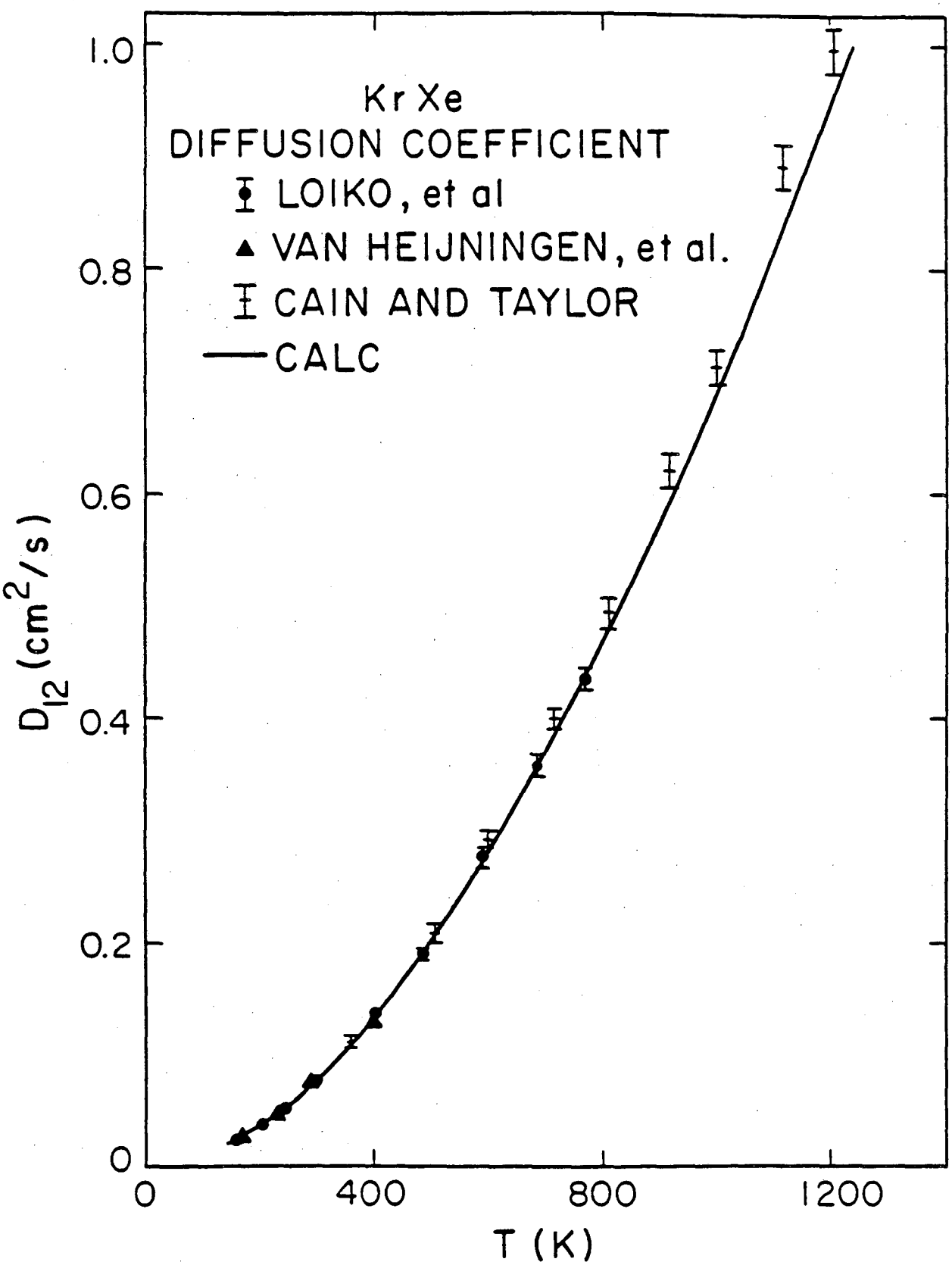
Kr Xe
DIFFUSION COEFFICIENT
LOIKO, et al
VAN HEIJNINGEN, et al.
CAIN AND TAYLOR
CALC
1.0
0.8
0.6
0.4
0.2
0
D_{12} (cm^2/s)
0
400
800
1200
T (K)

Fig. 12.

This report was done with support from the Department of Energy. Any conclusions or opinions expressed in this report represent solely those of the author(s) and not necessarily those of The Regents of the University of California, the Lawrence Berkeley Laboratory or the Department of Energy.

Reference to a company or product name does not imply approval or recommendation of the product by the University of California or the U.S. Department of Energy to the exclusion of others that may be suitable.

TECHNICAL INFORMATION DEPARTMENT
LAWRENCE BERKELEY LABORATORY
UNIVERSITY OF CALIFORNIA
BERKELEY, CALIFORNIA 94720